Applied Surface Science 277 (2013) 111–120

Contents lists available at SciVerse ScienceDirect

Applied Surface Science

journal homepage: www.elsevier.com/locate/apsusc

Photoactive layer-by-layer films of cellulose phosphate and titanium dioxide containing phosphotungstic acid

Sajjad Ullah[a], José Javier Sáez Acuña[b], André Avelino Pasa[c], Sara A. Bilmes[d], Maria Elena Vela[e], Guillermo Benitez[e], Ubirajara Pereira Rodrigues-Filho[a,*]

[a] Instituto de Química de São Carlos, Universidade de São Paulo, PO Box 780, São Carlos, São Paulo 13564-970, Brazil
[b] Centro de Ciências Naturais e Humanas, Universidade Federal do ABC, Santo Andre, Sao Paulo, 09210-170, Brazil
[c] Surface and Thin Film Laboratory, Physics Department, Federal University of Santa Catarina, PO Box 476, Florianópolis, SC 88040-900, Brazil
[d] Universidad de Buenos Aires, Facultad Ciencias Exactas y Naturales, Instituto de Química Física de los Materiales, Medio Ambiente y Energía – INQUIMAE, Ciudad Universitaria, Pab. 2, Buenos Aires C1428EHA, Argentina
[e] Laboratorio de Nanoscopías y Fisicoquímica de Superficies, Instituto de Investigaciones Fisicoquímicas Teóricas y Aplicadas (INIFTA), Universidad Nacional de La Plata – CONICET, diagonal 113 esquina 64. C.C.16.Suc.4, 1900 La Plata, Argentina

ARTICLE INFO

Article history:
Received 5 February 2013
Received in revised form 14 March 2013
Accepted 3 April 2013
Available online 12 April 2013

Keywords:
Cellulose phosphate
Layer-by-Layer
Titania
Phosphotungstic acid
Photocatalysis
Photochromism

ABSTRACT

A versatile layer-by-layer (LbL) procedure for the preparation of highly dispersed, adherent and porous multilayer films of TiO_2 nanoparticles (NPs) and phosphotungstic acid (HPW) on a variety of substrates at room temperature was developed based on the use of cellulose phosphate (CP) as an efficient and non-conventional polyelectrolyte. UV/vis absorption spectroscopy confirmed the linear and regular growth of the films with the number of immersion cycles and a strong adsorption ability of CP towards TiO_2 NPs. FTIR spectroscopy showed that HPW binds to the surface of TiO_2 through the oxygen atom at the corner of the Keggin structure. XPS results showed that the interaction between TiO_2 and CP is through Ti–O–P linkage. A model is proposed for the TiO_2–HPW interaction based on XPS and FTIR results. FEG/SEM study of the surface morphology revealed a porous film structure with a homogenous distribution of the TiO_2 NPs induced by CP. HRTEM studies showed that the resulting composite films consist of crystalline anatase and rutile phases and poly-nano-crystalline HPW with a semi-crystalline TiO_2–HPW interface. These CP/TiO_2 and CP/TiO_2/HPW LbL films showed good photoactivity against both saturated and unsaturated species, for instance, stearic acid (SA), crystal violet (CV) and methylene blue (MB) under UV irradiation. The CP/HPW films formed on bacterial cellulose (BC) showed good photochromic response which is enhanced in presence of TiO_2 due to an interfacial electron transfer from TiO_2 to HPW. This simple and environmentally safe method can be used to form coatings on a variety of surfaces with photoactive TiO_2 and TiO_2/HPW films.

1. Introduction

TiO_2 is a wide band-gap semiconductor with extensive use in pollutants remediation as a photocatalyst [1] and other applications such as self-cleaning devices [2], superhydrophilic coatings [3], nanoparticles-coated facemasks to protect against infectious agents [4] and antibacterial coatings on medical devices [5]. Another important use of TiO_2 layers is in energy generation; two energy generation devices based on TiO_2 have attracted the attention: (a) dye sensitized photovoltaic devices [6] and (b) bio-photo-fuel cells based on biomass degradation [7].

Most of these applications demand the formation of uniform and porous TiO_2 layers. Therefore, the study of methodologies to form homogenous layers of TiO_2 on different substrates under soft conditions is of great interest. The aim of this work was to study the viability of the use of LbL approach [8] as a soft and affordable procedure to form the mixed anatase/rutile NPs thin films on a variety of substrates using CP as a promising polyelectrolyte. Though the LbL method has the advantages of simplicity, flexibility, low-cost instrumentation and low temperature deposition, it usually requires modification of the substrate's surface to improve adherence of NPs and a longer film deposition time since the amount of the NPs adsorption per deposition cycle is usually low. To overcome the problem of low adsorption, we need a polyelectrolyte or some molecular binder to bind TiO_2 NPs together and at the same time to the substrate on which the film is grown. Many binders, both molecular and polymeric, have been used for this purpose such as poly(diallyldimethylammonium chloride), PDDAC [9], poly(acrylic acid), PAA [10], titanium (IV) bis(ammonium lactato) dihydroxide, TALH [11] and phytic acid, PA [12]. However,

* Corresponding author. Tel.: +55 1633739439; fax: +55 1633739982.
E-mail addresses: uprf@iqsc.usp.br, biraprfilho@yahoo.fr (U.P. Rodrigues-Filho).

0169-4332/$ – see front matter © 2013 Elsevier B.V. All rights reserved.
http://dx.doi.org/10.1016/j.apsusc.2013.04.011

the use of most of these polyelectrolytes either requires a strict pH-control of both polyelectrolyte solution and nanoparticles suspension or lack universality with respect to the type of substrates being used. For example, PDDAC, a cationic polyelectrolyte, can be used to form $(PDDAC/TiO_2)_n$ LbL films on quartz by adjusting pH of PDDAC solution to 6.4 and TiO_2 dispersed in a pH 10 carbonate–hydrogencarbonate buffer solution [9]. Similarly, poly (acrylic acid) (PAA), a weak anionic polyelectrolyte has been used to form LbL films of TiO_2 on cellulose acetate nanofibers but again such deposition require pH-adjustment of both PAA and TiO_2 to 2.5 [10]. Kim et al. observed that the thickness and roughness of $(TiO_2/TALH)_n$ LbL films were highly sensitive to a change in pH of TALH [11]. Phytate, an inositol poly-phosphate, has also been used as a molecular binder to build nanostructured TiO_2 films by LbL method on ITO [12] and thiol-modified gold electrodes at pH 3 [13]. However, the use of phytate as a binder lacks universality. Thus a best binder is one which reduces the deposition time and/or number of steps involved and can be applied on a variety of substrates. In this study, the polyelectrolyte chosen was CP, a phosphoric ester of cellulose which can act as chelate [14] toward transition metals in a similar fashion as phytate [15]. However, unlike phytate, the use of aqueous suspension of CP does not require any pH-adjustment and rapid deposition of TiO_2 NPs occurs into films formed on CP-modified substrates. Moreover, cellulose is a polymer, so it can fold all over the nanoparticles improving their dispersion on different substrates. We are going to demonstrate the ability of CP as a binding and dispersing agent for mounting photoactive TiO_2 LbL films on glass, quartz, silicon and bacterial cellulose. Furthermore, polyoxometalates such as HPW find wide application in preparation of photochromic and photocatalytic materials [16–18]. They accept electrons without significant structural changes to yield mixed valence coloured species (heteropolyblues or heteropolybrowns) useful for photochromic application while the generation of OH radical from the reaction of the excited catalyst (HPW) with H_2O upon UV illumination make them important photocatalyst [19,20]. Since, the combined use of HPW and TiO_2 is advocated to improve the quantum yield of the TiO_2 photoactivity [21] and photochromic response of HPW [22–24], based on the fact that the transfer of electron form the conduction band of TiO_2 to HPW is thermodynamically favourable [21], which on one hand can decrease the electron–hole (e^-–h^+) recombination in TiO_2 and on the other hand can assist in the photoreduction of HPW. Thus photochromism and photoactivity of TiO_2/HPW system has close connection. Here, we also report the formation of nanocomposite LbL films of HPW and TiO_2, $(CP/TiO_2)_n$/HPW, with photocatalytic and photochromic properties using CP as binder. The method for the preparation of such multilayers nanocomposite films based on the use of CP as a binder offers the greater advantages of generality, versatility and practicality since it can be used to form multilayer films of the desired thickness on almost all substrates in a very short time and involves the use of more environmentally safe reagents.

2. Materials and methods

2.1. Chemicals

Phosphotungstic acid hydrate ($H_3PW_{12}O_{40}{\cdot}nH_2O$), cellulose phosphate (fine mesh), and Titanium dioxide (10% (wt/vol.) dispersion in water) were purchased from Sigma–Aldrich (USA) and used without any modification or purification. Crystal violet ($C_{25}N_3H_{30}Cl$) was supplied by QHEMIS (SP, Brazil) and stearic acid (SA) was obtained from Labsynth (SP, Brazil). Bacterial cellulose (BC) membranes were from BioFill (Curitiba, Brazil) and cotton quantitative filter paper (MN 640 m) was obtained from Macherey–Nagel (Germany).

2.2. Films preparation

The multilayer $(CP/TiO_2)_n$ and $(CP/TiO_2)_n$/HPW films were prepared using the versatile LbL assembly technique employing a disc elevator MA-765 Marconi (Piracicaba, SP, Brazil). The general procedure for all film preparations was to prepare a 0.1% (unless otherwise specified) suspension of TiO_2 and 0.1% suspension of CP separately, followed by sonication in an ultrasonic bath for 1 h at room temperature. Only the supernatant layer of CP was used for films preparation. The HPW solution was prepared by adding the weighed amount of HPW to an aqueous solution already adjusted to pH ~ 1 with $HClO_4$ to avoid decomposition of the polyanion into its lacunary compounds [25]. The substrates (quartz, glass plate, Si wafers) were cleaned before use by immersing in Piranha solution (2:1 mixture of H_2SO_4 and H_2O_2) and heating at 90 °C for 1.5 h followed by rinsing with copious amount of distilled water and drying in a stream of nitrogen. The whole film formation process consisted of (i) surface modification of the substrate and (ii) formation of the films on modified surface. Surface modification step consisted of two immersions, of 2 min each, of the substrate in CP suspension. The onward film formation procedure consisted of a sequence of immersion steps of the CP-modified substrates in (a) TiO_2 suspensions for 2 min and (b) CP suspension for 10 s, and the cycle repeated n-times to obtain multilayers $(CP/TiO_2)_n$ films. Finally a single immersion of the $(CP/TiO_2)_n$ films in HPW solution (40 mM, unless otherwise specified) was carried out to complete the film formation. The photochromic CP/HPW and CP/HPW/TiO_2 films formed on bacterial cellulose (BC), and discussed in Section 4, were prepared by two immersion of BC in CP, followed by one immersion of 2 min in HPW solution and one immersion in 0.05% TiO_2 suspension. In all cases, the immersion and withdrawal speed of the disc elevator was adjusted to 150 mm min^{-1} and a drying interval of 90 s was used between each two immersions in TiO_2.

2.3. Characterisation techniques

UV/Vis Spectra of the films on quartz plates (UQG Optics, UK) were obtained using HP 8452A diode array single beam spectrophotometer (Hewlett Packard, USA). Absorption FTIR spectra in the range 400–4000 cm^{-1} at a spectral resolution of 4 cm^{-1} were acquired for the films on Si windows (UQG Optics, UK) with an MB-102 (Bomem, Canada) spectrometer. Raman spectra of the films formed on cotton quantitative filter paper and BC were collected with a LabRAM HR 800 model Raman Spectrophotometer (Horiba Jobin Yvon) equipped with a camera and CCD detector (model DU420A-OE-325) and using a He–Ne laser (632.81 nm). The spectra were taken between 100 and 4000 cm^{-1} with acquisition time of 300 s, 3 cycles and slit size of 100 μm. SEM images were obtained using JEOL JSM-6701F Scanning Electron Microscope equipped with field emission gun (FEG-SEM) and ZEISS LEO 440 (Cambridge, England) Scanning Electron Microscope equipped with a tungsten filaments and SE Detector (model 7060, Oxford). For HRTEM study, films were formed by immersing the carbon-coated copper grid (CFC-200Cu, Electron Microscopy Sciences, USA) in respective suspensions. HRTEM images were obtained using a JEOL (JEM2100) transmission electron microscope operated at an accelerating voltage of 200 kV and equipped with a LaB_6 electron gun and an Energy-Dispersive X-ray (EDX) detector. The TEM image analysis was performed using the Gatan's Digital micrograph image processing programme. X-ray photoelectron spectroscopy (XPS) data were collected using a non-monochromatic Al Kα source (1486.6 eV) XR50, Specs GmbH and a hemispherical electron energy analyzer PHOIBOS 100, Specs GmbH operating at 40 eV pass energy for survey spectra and 20 eV for narrow scans. A two-point calibration of the energy scale was performed using sputtered cleaned gold (Au 4f7/2, binding energy (BE) = 84.00 eV) and copper (Cu 2p3/2,

BE = 932.67 eV) samples; the photoelectron take-off angle was 90°. Sample films were prepared by dip-coating on single crystal silicon as mentioned in Section 2.2. The charge correction was made with respect to Si2p line at 99.15 eV. Spectra fitting was performed using XPSPeak 4.1 (http://www.uksaf.org/software.html#1) using a Shirley type background and a product of Gaussian and Lorentzian functions for the peaks. Quantitative analysis was performed taking into account the Scoffield cross sections for each element.

2.4. Photocatalytic experiments

The photocatalytic activity of the $(CP/TiO_2)_n$ and $(CP/TiO_2)_n$/HPW films formed on different substrates was tested by measurement of the area under the absorbance peaks of stearic acid (SA), crystal violet (CV) and methylene blue (MB) after each irradiation step with ultraviolet (UV) light in the presence of the photoactive films. To estimate the direct photolysis, a control experiment was run in each case, by exposing the target species (MB, CV and SA) directly to UV light and recording the change in area/absorbance of their respective peaks in absence of photoactive films.

The UV radiation was delivered by 16S Solar Light Simulator (Solar Light Co., USA) with an automatic shutter and internal filter was used in conjunction with a PMA2100 radiometer equipped with PMA 2110 UVA and PMA 2106 UVB detectors. The Solar Light Simulator delivers a maximum power of 150 W; the lamp-to-sample distance was around 7 cm in case of CV and MB and 11 cm in case of SA photodegradation; the UV-spot size was around 1.0 cm in case of CV and MB and 1.5 cm in case of SA.

2.4.1. Photodegradation of stearic acid

To study the photocatalytic degradation of SA by the hybrid films, 10 μL of 30 mM solution of SA in ethanol was applied as a thin layer on the surface of the photoactive CP/TiO_2 and CP/TiO_2/HPW films prepared on silicon wafer and left to dry for 2 h. FTIR spectra were recorded before and after UV irradiation doses to monitor the change in absorbance and hence peak area of the SA absorption peaks (2800–3000 cm^{-1}) assigned to stretching mode of the CH_3 and CH_2 groups. Unlike CV, the stearic acid over-layer was irradiated directly from the front.

2.4.2. Photodegradation of crystal violet

The photocatalytic tests were performed by spreading 5 μL of 0.1% CV in order to form a layer on only one of the two surfaces of the hybrid films (HF) on quartz. Then UV/vis absorption spectra of the film/CV assembly were taken before and after UV irradiation doses (total UV dose ~12.6 J cm^{-2} = 30 min). To minimize the possibility of direct photolysis of CV by UV irradiation, the sample films were irradiated from the backside onto the face uncoated with CV, allowing the UV to pass through the film before reaching the CV layer (scheme S1 in supplementary information). The photoactivity of the films was evaluated by monitoring the decrease in absorbance (peak area) of the CV band (460–800 nm).

2.4.3. Photodegradation of methylene blue

3 mL of 5 ppm solution of MB was placed in a quartz cuvette and the films formed on BC and/or quartz were immersed in this solution and UV/vis spectra were taken before immersion, after 5 min of immersion and after various irradiation doses.

2.5. Photochromism experimental set-up

The photochromic response of the CP/HPW and $CP/HPW/TiO_2$ films formed on bacterial cellulose (BC) was measured as function of UV irradiation delivered by the 16S Solar Light Simulator already described in Section 2.4. The absorbance of the films at λ_{max} for the reduced blue form of HPW was measured as function of irradiation time to evaluate the photochromic behaviour of HPW in presence and absence of TiO_2. The UV lamp was placed close to the spectrophotometer and electronic spectra taken without any significant time delay to ensure precise measurement without any significant leaching of blue colour of the reduced HPW.

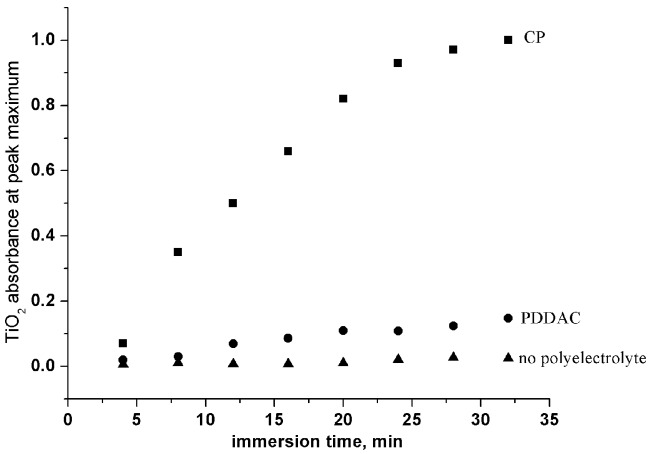

Fig. 1. Comparison of the amount of TiO_2 adsorbed onto quartz plates from a 0.05% TiO_2 suspension, as measured by an increase in TiO_2 absorbance, when no polyelectrolyte is used (▲) when PDDAC is used (●) and when CP is used (■) as binder between surface of the substrate and TiO_2 NPs and between TiO_2 layers.

3. Results and discussion

3.1. Monitoring of the film formation by electronic spectroscopy

UV/vis spectroscopy was used to monitor the film growth on quartz in presence of CP and PDDAC each. The absorbance due to $O^{2-} \rightarrow Ti^{4+}$ ($O2p \rightarrow Ti3d$) ligand-to-metal charge transfer band of TiO_2 at around 330 nm [26,27] increases almost linearly with the deposition cycles which is characteristic for a regular growth of the films (Fig. 1). The complete UV/vis spectra of the corresponding $(PDDAC/TiO_2)_{16}$ and $(CP/TiO_2)_{16}$ films are shown in Fig. S1. It can be noted from Fig. 1 that the increase in absorbance of TiO_2 at around 330 nm and hence the amount of TiO_2 adsorbed into the multilayer films per deposition cycle is far greater when CP is used as a binder.

The better adsorption of TiO_2 by CP in LbL films suggests higher affinity of CP for TiO_2 and hence its better binder ability, possibly because of H-bond interaction between TiO_2 and CP [28] or Ti–O–P bond formation. Moreover, Cellulose phosphate has higher adsorption affinity for the Pearson's "hard acid" sites on TiO_2 surface (Ti^{4+}) because of the presence of the hard base, PO_4^{3-} group [29].

3.2. Monitoring of the films formation by Infrared absorption spectroscopy

Since HPW shows four distinct vibrational modes in IR region, FTIR absorption spectroscopy was used to monitor the film growth and interaction between film components, especially TiO_2 and HPW. Upon immersion of the substrate in TiO_2 suspension, a broad band appears between 870 and 670 cm^{-1} (Fig. 2A). This absorption band, which increases with the number of deposition cycles, can be assigned to the stretching modes of Ti–O and Ti–O–Ti groups in the TiO_6 octahedral of the TiO_2 structure where the Ti–O mode (768 cm^{-1}) is observed as a shoulder on the Ti–O–Ti mode [30,31].

The presence of HPW characteristic bands in the FTIR spectra at 1076, 978, 911 and 800 cm^{-1} correspond to $P—O_a$, $W=O_d$,

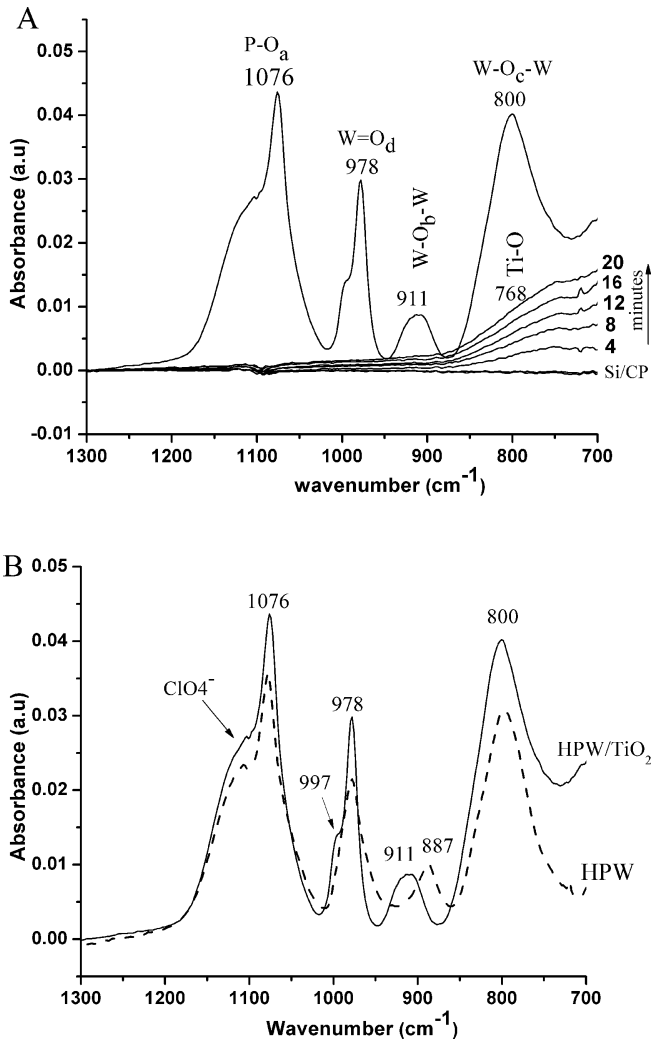

Fig. 2. (A) Infrared absorption spectra of hybrid $(CP/TiO_2)_{10}$ film on silicon wafer as a function of CP/TiO_2 bilayers deposition and with HPW adsorbed as a last upper layer, (B) bare HPW layer (no CP or TiO_2 present) deposited on silicon wafer from HPW solution containing $HClO_4$ to adjust pH ~ 1 (dashed line) and CP/TiO_2/HPW hybrid film (solid line).

W—O_b—W, W—O_c—W vibrational modes in the Keggin structure, respectively. Thus, it confirms HPW adsorption on the CP/TiO_2 multilayer films and preservation of the Keggin structure in the hybrid films [32]. Since free ClO_4^- shows anti-symmetric stretching mode ν_{as}(Cl—O) at 1092 cm^{-1}, the shoulder of the PO_4 band at 1076 cm^{-1} in the hybrid films was assigned to the presence of adsorbed ClO_4^- [33]. Despite similar, the band positions for the bare HPW and the one in the CP/TiO_2 films are not the same; the W—O_b—W mode in the hybrid film is blue-shifted by about 24 cm^{-1} and the W=O_d is broadened (Fig. 2B). Both features can be interpreted as due to the interaction of the $[PW_{12}O_{40}]^{3-}$ unit with the TiO_2 surface as suggested by Pearson et al. [34] or to the interaction with phosphate groups in CP. To verify this, we compared the spectra of the bare HPW film on silicon wafer, HPW on CP-modified Silicon wafer, HPW on TiO_2 film without CP, and HPW in the CP/TiO_2 multilayer film (Fig. S2). From Fig. S2, it becomes clear that the upward shift in the W—O_b—W mode is only observed when TiO_2 is present. These results confirmed that the phosphotungstate is interacting with the titania through oxygen atom (W—O_b—W) at the corner of Keggin structure and this interaction is further explored using XPS analysis discussed later in the text.

3.3. Characterization of the hybrid films on cellulose substrates by Raman spectroscopy

Infrared spectroscopy of the hybrid films in cellulose substrates is complicated due to strong absorption by the cellulose functional groups which overlap with the inorganic absorption bands from TiO_2. On the other hand, Raman Spectroscopy is more sensitive to TiO_2 vibrational modes than to the cellulose vibrational modes; therefore, it was used to confirm the phase identity and anchoring of TiO_2 NPs onto cotton fibres in the hybrid films formed on cellulose. A comparison of the Raman spectra of the pure and film-modified cellulose fibers (Fig. S3) shows that new bands arise at 143, 196 and 640 cm^{-1} in spectrum of the modified fibers all of which are assigned to anatase TiO_2 [35–38]. Raman spectroscopy is thus helpful in confirming the anchoring and identifying the phase of TiO_2 NPs onto cellulose fibres at the outset of the experiment before switching to the more sophisticated SEM and TEM techniques.

3.4. Physical surface characterization of the films

SEM, FEG/SEM and HRTEM studies of the films formed on different substrates (single crystal Si (1 1 1), glass, quartz, quantitative cellulose filter paper, and bacterial cellulose) were carried out to get information on the morphology, nanostructure, particle size distribution and the interface between TiO_2 and HPW.

3.4.1. SEM and FEG-SEM studies of the films

The surface microstructure of the multilayer thin films deposited on different substrates was investigated by SEM and FEG-SEM.

Fig. 3A and B shows the SEM image of the pure and TiO_2-modified fibres of filter paper cellulose, respectively. It can be seen that the fibres of filter paper cellulose are larger than those of BC (Fig. 3C) and TiO_2 NPs form a uniform thin layer on cellulose fibres indicated with arrows. Though there is some aggregation of TiO_2 NPs, the presence of CP layer on the surface results in more uniform distribution of TiO_2 NPs as shown by Ti X-ray mapping in the presence and absence of CP in cellulose/TiO_2 films (Fig. 4). The FEG/SEM image of pure BC (Fig. 3C) shows a network of densely packed nanometric fibres which, because of their high surface area and porous structure, can be used a suitable template for incorporation of TiO_2 NPs [39]. Fig. 3D presents an FEG/SEM low magnification image of the uniformly distributed CP/TiO_2 films formed on BC. There is some agglomeration of TiO_2 NPs due to the cavities and non-planar surface of BC membrane. The high magnification image (Fig. 3F) shows that TiO_2 particles of around 56 nm average size are adsorbed onto the surface of BC microfibrils. The multilayers deposition seems to result in a vertical growth of the film and agglomeration of NPs (Fig. 3E). A similar growth pattern can be observed in TiO_2/CP films deposited on single crystal silicon (Fig. 5C and D). This feature results in the formation of highly porous films which can offer high accessibility to foreign particles, pollutants and microorganisms.

The $(CP/TiO_2)_n$ films formed on quartz also exhibit good distribution of TiO_2 NPs (Fig. 5). The SEM analysis thus point out CP as a good dispersant of TiO_2 NPs to form porous uniform films on a variety of substrates.

3.4.2. TEM and HRTEM study of the films

Fig. 6 shows the TEM images of the CP/TiO_2 (A) and CP/TiO_2/HPW (B) films. It can be seen that TiO_2 NPs are spherical in shape and show some degree of polydispersity. An analysis of histogram (Fig. S4) of TiO_2 NPs showed that the average particle size of TiO_2 NPs in CP/TiO_2 films is around 50 nm and this particle size of TiO_2 NPs is preserved in the films containing HPW. HPW particles in these

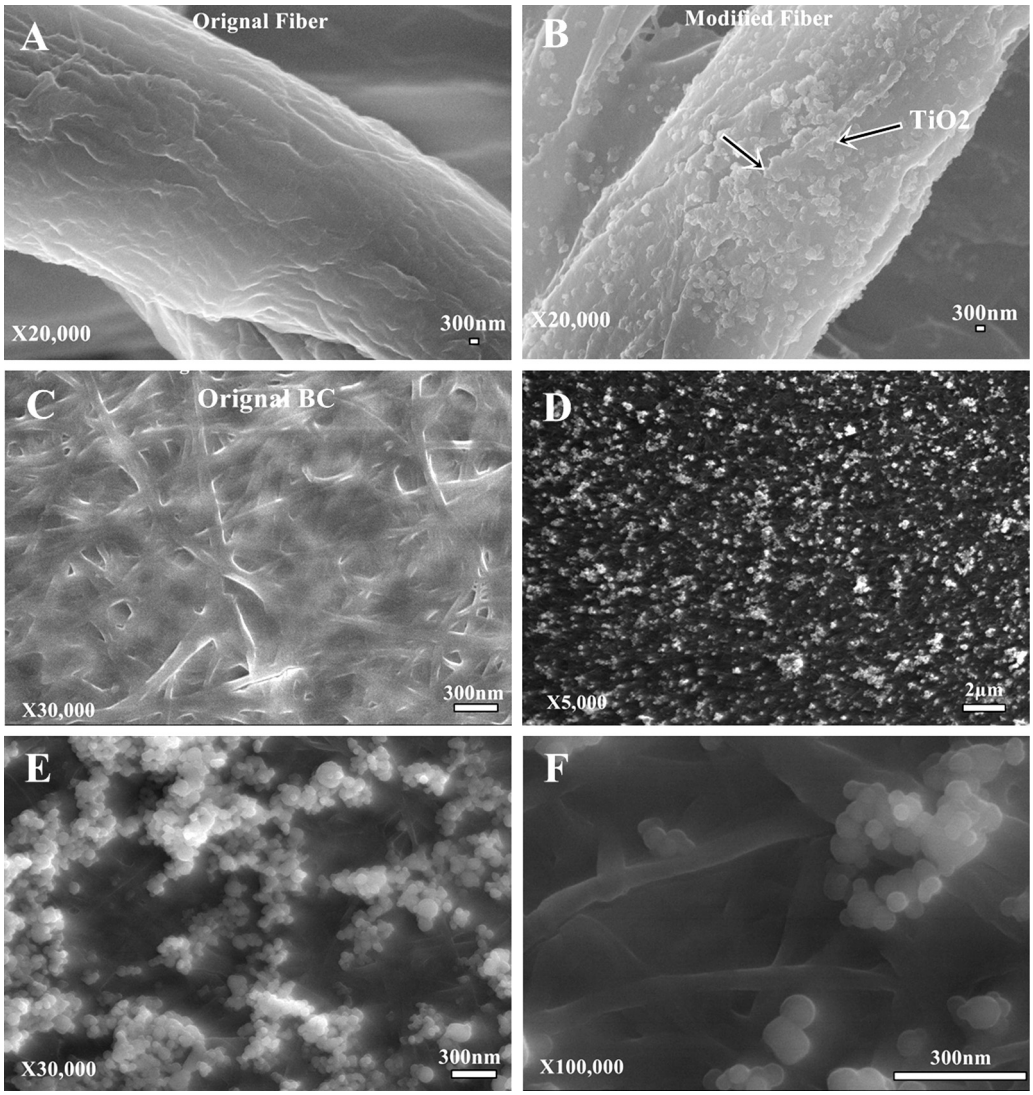

Fig. 3. SEM images of unmodified fibers of cellulose filter paper (A) and after formation of CP/TiO_2 film (B), FEG/SEM image of original BC membrane (C) and after formation of CP/TiO_2 film on BC in low (D) and high magnification (E and F).

films have a bimodal size distribution, the larger particles being 150–200 nm and the smaller ones are around 32 nm in diameters.

In order to differentiate between TiO_2 and HPW particles and make the histograms, we carried out nano-EDS analysis, with electron beam focused in the form of a spot of about 15 ± 3 nm diameter, of a sufficiently large number of particles in a transmission electron microscope equipped with an EDX spectrometer. The EDS analysis showed that perfectly round smooth particles are those of TiO_2 while the roundish particles with irregular edges are those of HPW (Fig. 7).

The HRTEM images of the sample showed that the films consist of crystalline TiO_2 in both anatase and rutile phase (Figs. 6C and 8) while HPW shows poly-nano-crystalline behaviour, i.e. crystallites of a few nanometers randomly ordered (Fig. 6D). The interplanar distances (IPDs) on the HRTEM images of TiO_2 and HPW were measured and compared with data from Inorganic Crystal Structure Database (ICSD) [Rutile: collection code 51930; Anatase: collection code 154609; HPW collection code 904]. The measured values ($\pm$0.03) of IPD_S are 3.5, 2.35, 2.42 Å which correspond to (1 0 1), (0 0 4) and (1 0 3) planes of anatase [40] while the IPDs values ($\pm$0.03) of 2.30 and 2.07 Å correspond to the (2 0 0) and (2 1 0) plane of rutile phase [41]. The IPDs values ($\pm$0.03) encountered for HPW are 3.63, 3.77, 4.13, 4.46 and 5.1 Å which corresponds to the *h k l* values of (2 2 2), (3 1 1), (2 2 1), (2 2 0) and (2 1 1), respectively [42]. The bright field (BF) and dark field (DF) TEM images of the particles aggregates in the films are shown in Fig. 6E and F, respectively. These images were obtained by filtering only the electrons diffracted by (1 0 1) family of planes of TiO_2-anatase and (2 2 2) and (3 1 1) families of HPW. These TEM images show that most of the HPW and TiO_2 particles exist together in proper contact in these films, which also support the conclusion from FTIR analysis on interaction between HPW and TiO_2 (Figs. 2B and S2). The relatively large dark particles in (Fig. 6E) are of HPW, which are seen as diffusely bright in DF mode (Fig. 6F).

This is interesting to note as the brightness identifies the type of particle. Being crystalline, the TiO_2 NPs shine intensely brighter when viewed in the dark filed mode, whereas, HPW is neither completely crystalline nor completely amorphous; the form and type of brightness of HPW shows that it is composed of small nano-crystals co-existing with its amorphous form.

A detailed analysis of the interface between TiO_2 and HPW particles based on the HRTEM images showed that interface is semi-crystalline and is constituted by crystalline anatase and rutile phase of TiO_2 and poly-nano-crystalline HPW and small crystallites of HPW can be seen to grow as we go from interface towards the HPW (Figs. 8 and S5).

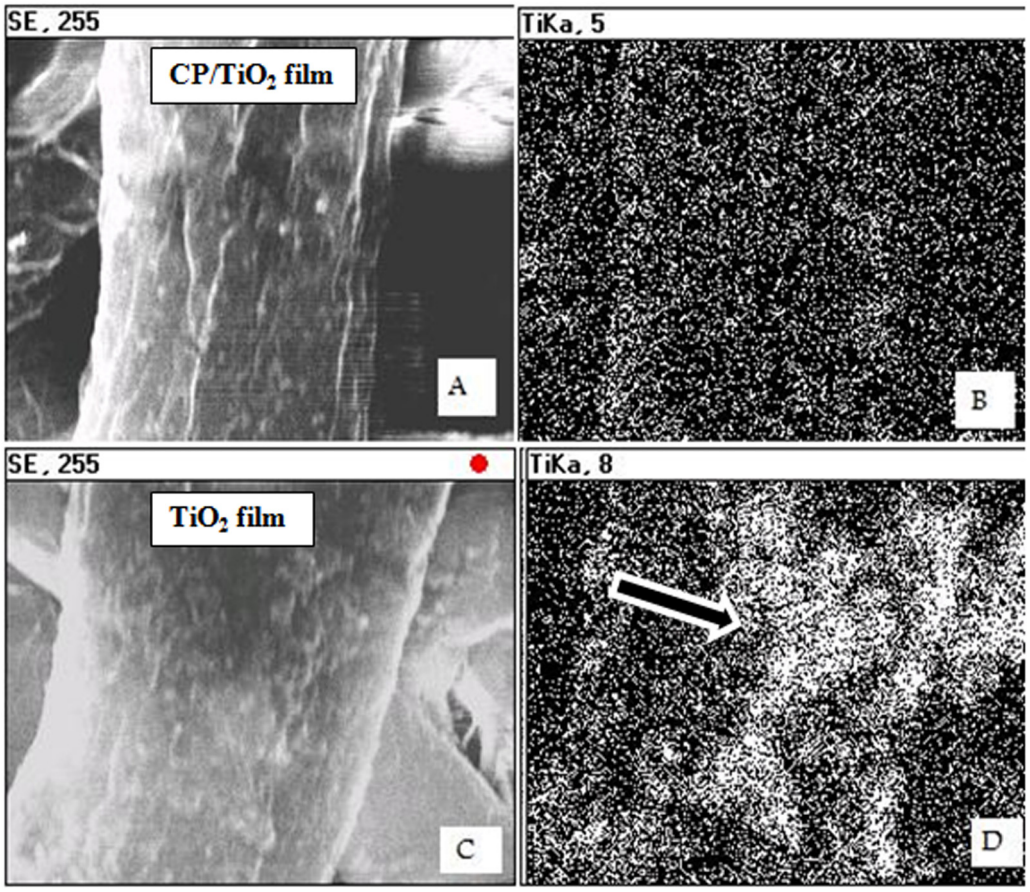

Fig. 4. Representative SEM images of TiO_2 modified-fibres (A and C) and the corresponding Ti X-ray mapping in the presence (B) and absence (D) of CP in filter paper cellulose/TiO_2 films; more agglomeration of TiO_2 NPs indicated with an arrow occurs in absence of CP (D).

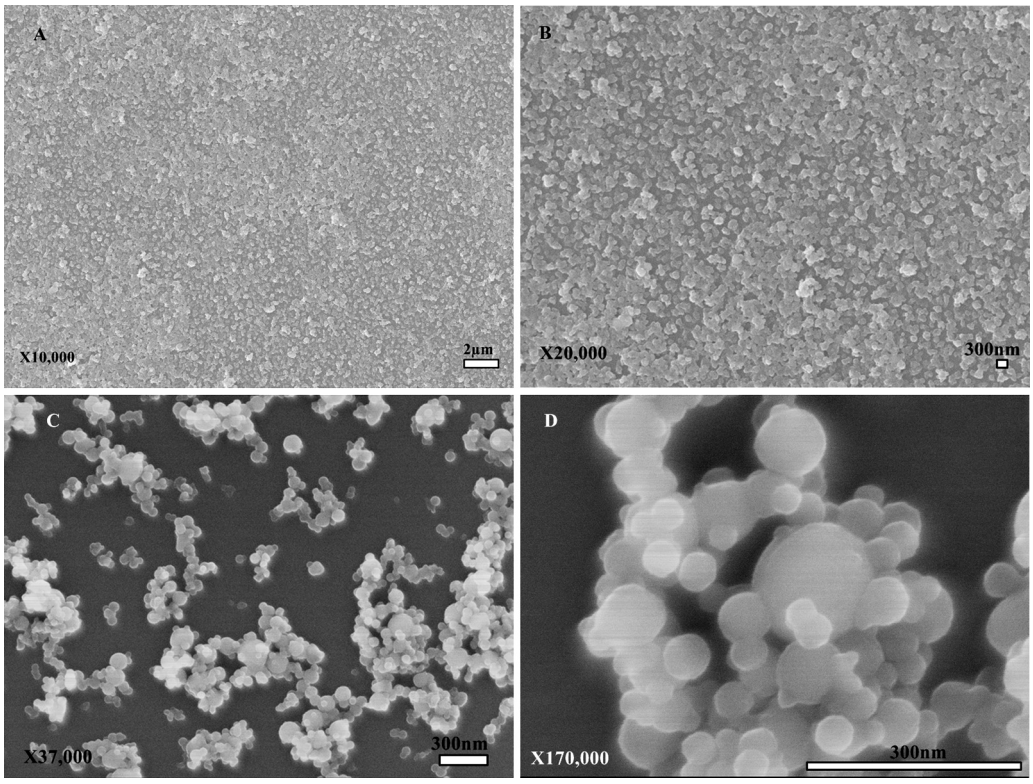

Fig. 5. SEM image of $(CP/TiO_2)_{10}$ film on quartz in low (A) and relatively high (B) magnification; FEG/SEM images of CP/TiO_2 film formed on single crystal silicon in low (C) and high (D) magnifications.

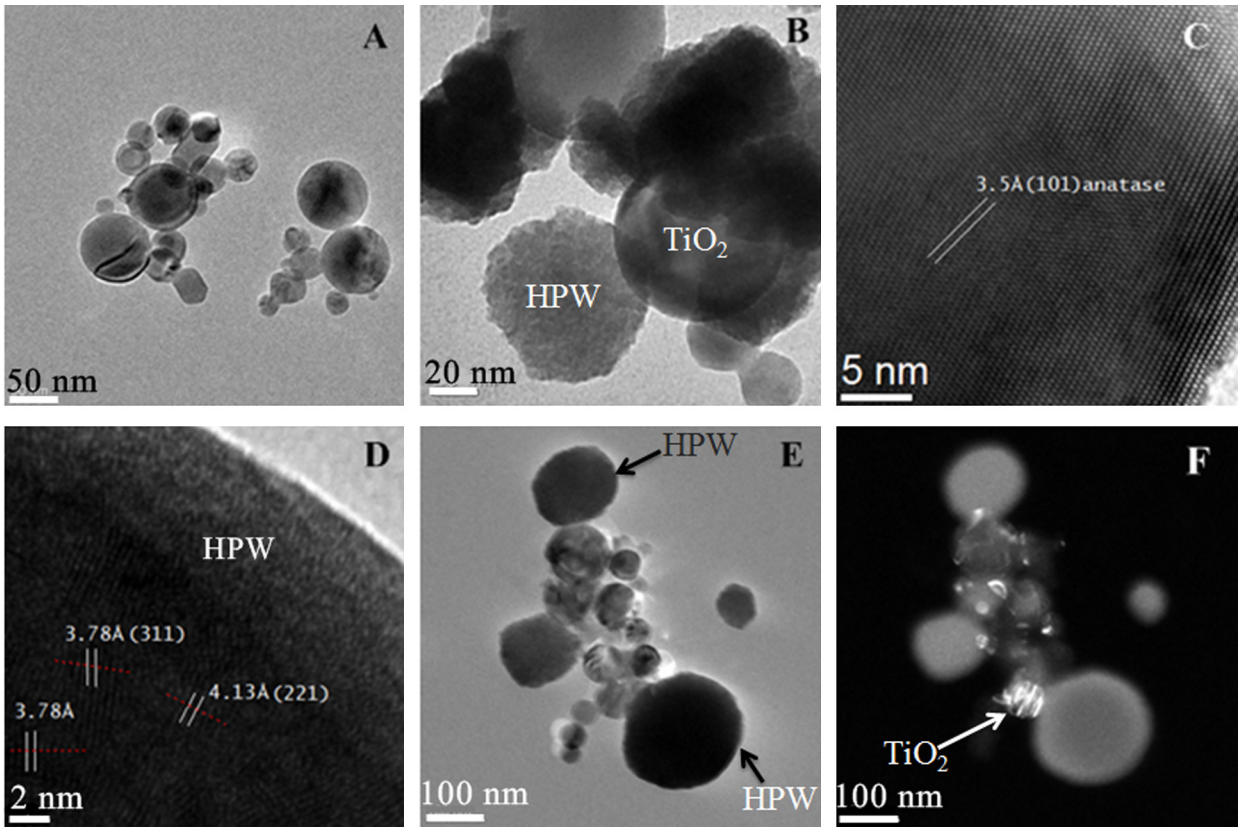

Fig. 6. TEM image of TiO_2 NPs (A), TiO_2 NPs and HPW particles in TiO_2/HPW film (B); HRTEM image of TiO_2 (C) and HPW (D) particles; Bright Field (E) and dark field (F) image showing the presence of and differentiating TiO_2 and HPW particles in TiO_2/HPW films.

3.5. Chemical surface characterization of CP/TiO_2/HPW films by X-ray photoelectron spectroscopy

The survey spectra of the films containing only CP, CP/TiO_2 and CP/TiO_2/HPW films are shown in Fig. S6. The XPS spectrum of CP films show the C1*s*, P2*p* and O1*s* XPS peaks at their characteristic BE values as identified in Fig. S6. The Si peaks are due to the support used. Ti2*p* and W5*d* peaks arise when TiO_2 and HPW are introduced into the films.

The high resolution Ti2*p* XP spectra exhibit the Ti2*p*3/2 peak at 458.4 eV for the CP/TiO_2 film (A) and 458.8 eV for the CP/TiO_2/HPW film (B) as shown in Fig. S7. Since pure anatase TiO_2 has Ti2*p*3/2 peak at BE of 458.1 eV, the Ti2*p*3/2 peak at 458.4 eV in (A) is assigned to the octahedrally coordinated Ti bound to CP, i.e. to the P–O–Ti linkage [43]. The 0.4 eV shift in the BE of Ti2*p*3/2 peak in going from CP/TiO_2 film to CP/TiO_2/HPW film indicates the interaction of HPW with CP/TiO_2 component of the film, in accordance with the data from FTIR analysis (Fig. 2B). However, almost no change is observed in O1*s* BE of TiO_2 in presence of HPW (Fig. 9).

The possible reason for this interaction may be explained as follows. Upon immersion of CP/TiO_2 film in the acidic HPW solution (pH ~ 1), the titania surface gets positively charged, which leads to an increase in BE of Ti2*p* peak. The positively charged titania electrostatically attracts the heteropolyanion $[PW_{12}O_{40}]^{-3}$ towards itself, leading to TiO_2–HPW interaction [44], while leaving no net effect on electron density around O atom of TiO_2 since this interaction, as well as a transfer of electron density from Ti to O, counterbalance the decrease electron density around O atom caused by protonation of titania (see Scheme 1). Thus we observe only a shift in Ti2*p* peak of titania and no change in O1*s* of Titania (Fig. 9).

The O1*s* spectra of CP film (A) shows a small intensity peak at lower BE side at around 530.9 eV which is close to BE of Na_2HPO_4 (531.0 eV) and hence could be assigned to the O1s of PO_4 unit of CP [45]. The main O1s peak of high intensity at around 532.3 eV is assigned to the O of cellulose unit [46,47]. The O1s peak at around 533.1 eV is assigned to the O of SiO_x species resulting from surface oxidation of Silicon substrate [48]. This peak decreases in intensity as TiO_2 and HPW layers are deposited on the substrate. In the XPS spectra of sample (B), in addition to the O1s of cellulose and SiO_x, a peak at 529.9 eV arises which is assigned to the O of the Ti–O–P bond of Titania–CP species [43]. This peak also decreases in intensity when HPW is deposited on surface of CP/TiO_2 film. Similarly, the O1s XP spectrum of CP/TiO_2/HPW film (C) can be resolved into 4 components, the new component that arise at 530.7 eV, in addition to those mentioned in (B), is due to O bound to W^{6+} of HPW [49] since the same value is observed for the $[NH_4]_{10}[W_{12}O_{41}]$ species [50] and H_2WO_4 [51] both of which has the O atom bound to hexavalent W^{6+} atom.

4. Photochromism of the CP/HPW/TiO_2 films

The HPW in these hybrid films formed on BC shows a quick response to UV irradiation and is photoreduced to form the blue coloured species which absorbs at around 480 nm (d–d transition) and 700 nm (intervalence charge transfer, IVCT) [17,20]. Two important things can be noted when TiO_2 is introduced into the BC/HPW film: Firstly, the absorbance and hence photochromic response of CP/HPW film is enhanced by about 35% in presence of TiO_2 (Fig. 10); secondly, the λ_{max} corresponding to IVCT is blue-shifted from 722 nm to 678 nm (Fig. S8).

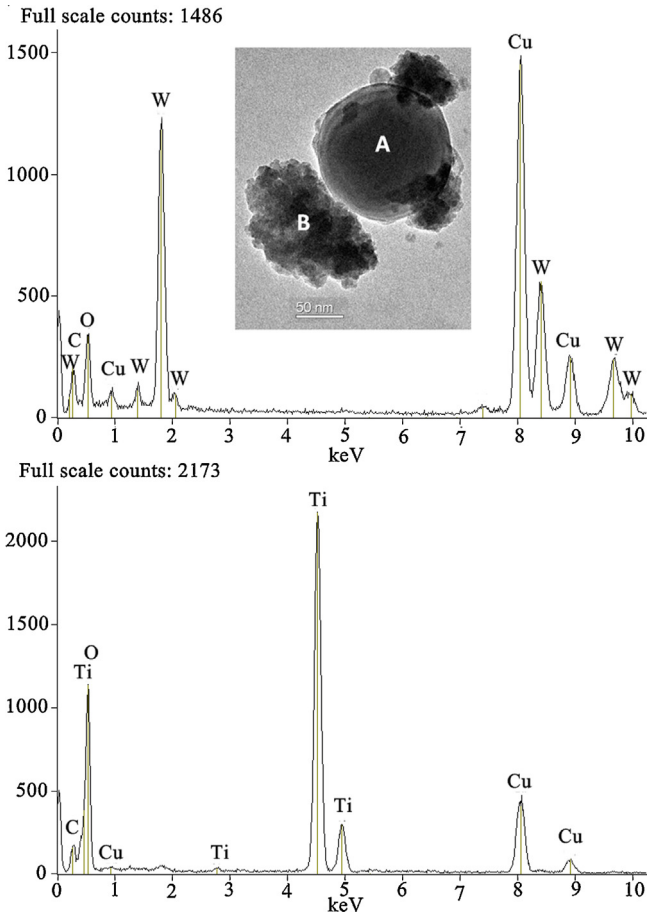

Fig. 7. EDS analysis of the selected particles aggregates shown as inset to identify their chemical identity. EDS spectrum of central round particle (marked A) is shown below, while EDS spectrum of rough-edged particle (marked B) is shown above.

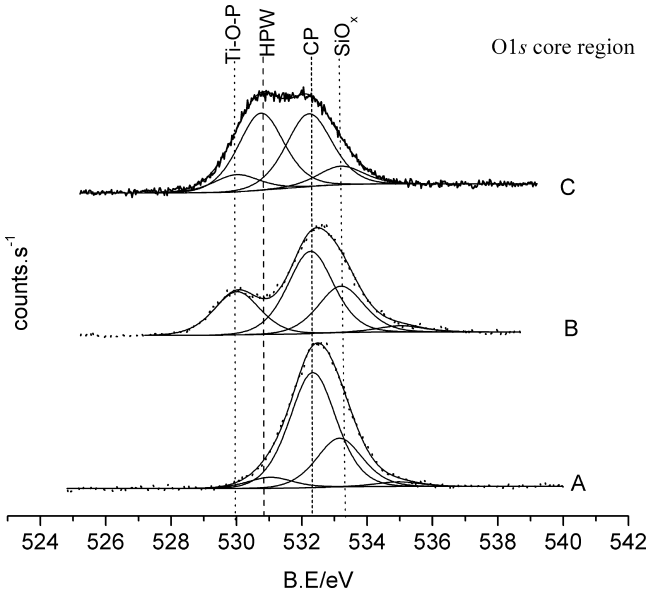

Fig. 9. O1*s* XP spectra of CP layer (A), CP/TiO_2 (B) and CP/TiO_2/HPW (B) films formed on silicon.

This increase in absorbance can be attributed to a transfer of photo-excited electron from the conduction bands of TiO_2 to HPW [20–22,52] thus leading to efficient reduction of HPW to its reduced blue form which absorbs visible light. The blue-shift of λ_{max} in presence of TiO_2 can be explained based on the fact that TiO_2 assists the two electron photoreduction of HPW [17].

5. Photocatalytic test

The CP/TiO_2 films with and without HPW showed good photoactivity against SA as measured by a sharp decrease in area of C—H stretching band of SA (Fig. S9). About 95% degradation of SA overlayer was observed within 12 min of UV irradiation (total dose of 5.0 J cm^{-2}). The introduction of HPW into the CP/TiO_2 films did not result in any significant increase in photoactivity of CP/TiO_2 films (Fig. 11). It was noted that a concentration of HPW higher than 1 mM leads to a decrease in photoactivity of CP/TiO_2 film.

It was inferred from Fig. 10 that as transfer of electron from TiO_2 to HPW results in an increase in photochromism, one should expect

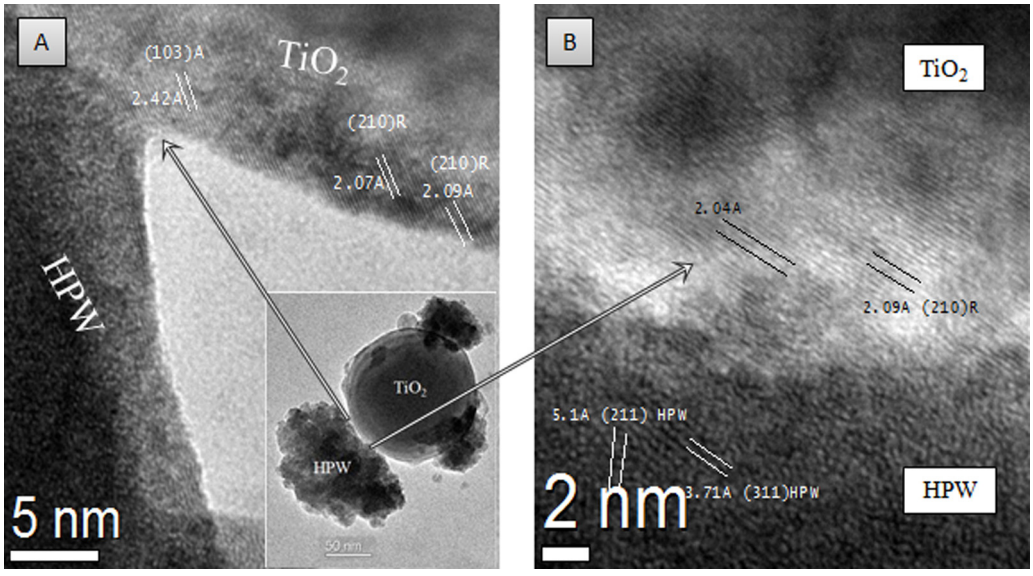

Fig. 8. HRTEM images showing the details of the interface between TiO_2 and HPW particle (shown as inset in A); HRTEM image of the edges of TiO_2 and HPW particle at the V-shaped inter-junction (A) and mid-region of the interface (B). The measured inter-planar distances corresponding to the (1 0 3) plane of anatase and (2 1 0) plane of rutile. The interface is semi-crystalline and consists of crystalline anatase and rutile phases of TiO_2 and poly-nano-crystalline HPW.

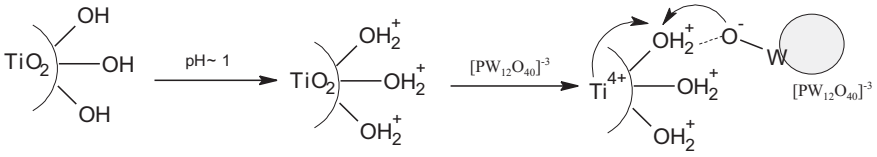

Scheme 1. Possible interaction between TiO_2 and HPW.

a low rate of electron–hole (e^-–h^+) recombination and increased photoactivity of TiO_2 [21,52]. We suggest that a possible decrease in exposed surface area of TiO_2 due to HPW deposited as a last layer on CP/TiO_2 films counteracts the effect of decrease in the rate of e^-–h^+ recombination and no net increase in photoactivity is seen. A decrease in e^-–h^+ recombination and increase in surface area of photocatalyst are thus essentials for increase in photoactivity. On the other hand, since photochromism is a bulk property and does not depend on surface properties, only electron transfer from TiO_2 to HPW is sufficient to increase the photochromism of HPW.

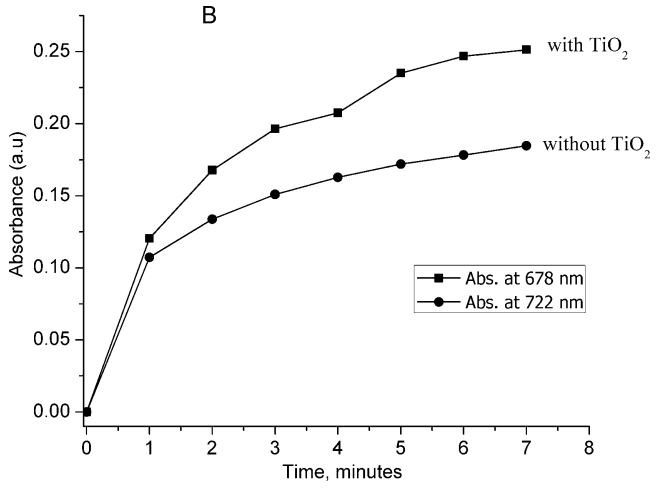

Fig. 10. Comparison of the photochromic response of CP/HPW film with and without TiO_2.

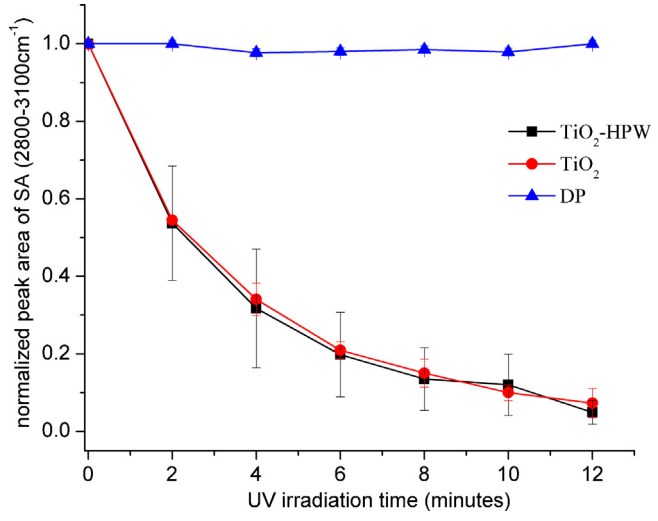

Fig. 11. Decrease in area of C—H stretching bands (2800–3000 cm^{-1}) of SA with time under UV irradiation in presence of CP/TiO_2 (●) and CP/TiO_2/HPW (■) films ([HPW] = 1 mM) and in absence of any photocatalytic film (▲) for a total irradiation time of 12 min (UV dose = 5.0 J cm^{-2}); direct photolysis (DP) of SA in absence of photocatalyst is almost negligible under experimental condition. Each point in the curve is an avergae of 3 independent measurements and the bars indicate standar deviation.

The CP/TiO_2 films formed on bacterial cellulose (BC) also showed good photoactivity under UV-illumination. About 50% of the MB was photodegraded within 30 min of irradiation (total UV dose ~15 J cm^{-2}) in the presence of BC/CP/TiO_2 films (Fig. S10). The same films formed on quartz also exhibited good photoactivity against MB (data not shown). The CP/TiO_2 and CP/TiO_2/HPW films exhibited good photodegradation of CV, but the introduction of HPW in the CP/TiO_2 films caused a decrease in CV photodegradation due to protonation of CV by the HPW since CV turned violet-to-yellow upon contact with HPW in the films [53] (Fig. S11). The CP/TiO_2 films degraded about 95% of CV within 30 min of UV irradiation whereas the direct photolysis of the CV layer by UV was only 3% for the same irradiation time (Figs. S11 and S12).

6. Conclusion

The results discussed above indicate that well-dispersed and uniformly distributed films of TiO_2 and TiO_2/HPW can be formed on a variety of substrates at room temperature by the simple dip-coating method employing cellulose phosphate (CP) as a non-conventional polyelectrolyte. CP has greater affinity for TiO_2 due to formation of Ti–O–P linkages between TiO_2 and CP. The interaction between TiO_2 and HPW in these hybrid films is through oxygen atom at the corner of HPW which arise from a combined electrostatic and H-bonding effect. The TiO_2 in the hybrid films is composed of crystalline anatase and rutile phases while HPW in these films shows poly-nano-crystalline behaviour. The CP/TiO_2 films formed on glass, quartz and BC showed good photoactivity while the CP/HPW/TiO_2 films formed on BC show enhanced photochromic behaviour. The combined used of TiO_2 and HPW in these film lead to an increase in photochromism of HPW but a higher concentration of HPW in the films suppress the photoactivity of TiO_2, possibly due a decrease in surface area of TiO_2. The method is simple, economic and environmentally safe and gives more practicality and versatility to the use of TiO_2 and HPW in various applications such as photocatalysis, photochromism as well as self-cleaning devices.

Acknowledgments

The Author, S. Ullah, thanks the Brazilian national council for scientific and technological development (CNPq-Brazil) and the Academy of sciences for the developing world (TWAS-Italy) for PhD fellowship and financial support. We acknowledge support from ANPCyT (Argentina, PICT-2010-2554, PICT-CNPQ 08-0019), UBACyT 20020100100636, CONICET GI-PIP 11220110101020. M.E.V. is researcher from CIC, Bs. As., Argentina, SAB is researcher of CONICET, Argentina. We also acknowledge the guidance, counseling and donation of bacterial cellulose as well as access to Raman spectrophotometer by Prof. Sidney J.L. Ribeiro from Instituto de Química, Universidade Estadual Paulista (UNESP), Araraquara, 14081-970, SP, Brazil.

Appendix A. Supplementary data

Supplementary data associated with this article can be found, in the online version, at http://dx.doi.org/10.1016/j.apsusc.2013.04.011.

References

[1] K. Hashimoto, H. Irie, A. Fujishima, TiO_2 photocatalysis: a historical overview and future prospects, Japanese Journal of Applied Physics 44 (12) (2005) 8269–8285.

[2] J.O. Carneiro, V. Teixeira, A. Portinha, A. Magalhães, P. Coutinho, C.J. Tavares, R. Newton, Iron-doped photocatalytic TiO_2 sputtered coatings on plastics for self-cleaning applications, Materials Science and Engineering: B 138 (2007) 144–150.

[3] R. Wang, K. Hashimoto, M. Chikuni, E. Kojima, A. Kitamura, M. Shimohigashi, T. Watanabe, Light-induced amphiphilic surfaces, Nature 388 (1997) 431–432.

[4] Y. Li, P. Leung, L. Yao, Q.W. Song, E. Newton, Antimicrobial effect of surgical masks coated with nanoparticles, Journal of Hospital Infection 62 (1) (2006) 58–63.

[5] P. Evans, D.W. Sheel, Photoactive and antibacterial TiO_2 thin films on stainless steel, Surface and Coatings Technology 201 (2007) 9319–9324.

[6] S. Ito, P. Chen, P. Comte, M.K. Nazeeruddin, P. Liska, P. Péchy, M. Grätzel, Fabrication of screen-printing pastes from TiO_2 powder for dye-sensitised solar cell, Progress in Photovoltaics: Research and Applications 15 (2007) 603–612.

[7] J. Nemoto, M. Horikawa, K. Ohnuki, T. Shibata, H. Ueno, M. Hoshino, Biophoto-fuel cell (BPFC) generating electrical power directly from aqueous solutions of biomass and its related compounds while photodecomposing and cleaning, Journal of Applied Electrochemistry 37 (2007) 1039–1046.

[8] G. Decher, Fuzzy nanoassemblies: toward layered polymeric multicomposites, Science 277 (1997) 1232–1237.

[9] J.-A. He, R. Mosurkal, L.A. Samuelson, L. Li, J. Kumar, Dye-sensitized solar cell fabricated by electrostatic layer-by-layer assembly of amphoteric TiO_2 nanoparticles, Langmuir 19 (2003) 2169–2174.

[10] B. Ding, J. Kim, E. Kimura, S. Shiratori, Layer-by-layer structured films of TiO_2 nanoparticles and poly(acrylic acid) on electrospun nanofibers, Nanotechnology 15 (2004) 913–917.

[11] J.-H. Kim, S. Fujita, S. Shiratori, Fabrication and characterization of TiO_2 thin film prepared by a layer-by-layer self-assembly method, Thin Solid Films 499 (2006) 83–89.

[12] K.J. McKenzie, F. Marken, Accumulation and reactivity of the redox protein cytochrome c in mesoporous films of TiO_2 phytate, Langmuir 19 (2003) 4327–4331.

[13] K.J. McKenzie, F. Marken, M. Oyama, C.E. Gardner, J.V. Macpherson, Electrochemistry in the presence of mesoporous TiO_2 phytate nanofilms, Electroanalysis 16 (2004) 89–96.

[14] D.M. Suflet, G.C. Chitanu, V.I. Popa, Phosphorylation of polysaccharides: new results on synthesis and characterization of phosphorylated cellulose, Reactive and Functional Polymers 66 (2006) 1240–1249.

[15] U.P. Rodrigues-Filho, Silvio Vaz Jr., M.P. Felicissimo, M. Scarpellini, D.R. Cardoso, R.C.J. Vinhas, R. Landers, J.F. Schneider, B.R. McGarvey, M.L. Andersen, L.H. Skibsted, Heterometallic manganese/zinc–phytate complex as a model compound for metal storage in wheat grains, Journal of Inorganic Biochemistry 99 (2005) 1973–1982.

[16] M.T. Pope, Heteropoly and Isopoly Oxometalates, Springer-Verlag, Berlin, 1983.

[17] E. Papaconstantinou, Photochemistry of polyoxometallates of molybdenum and tungsten and/or vanadium, Chemical Society Reviews 18 (1989) 1–31.

[18] M. de Oliveira Jr., A. Lopes de Souza, J. Schneider, U. Pereira Rodrigues-Filho, Local structure and photochromic response in Ormosils containing dodecatungstophosphoric acid, Chemistry of Materials 23 (2011) 953–963.

[19] P. Kormali, A. Troupis, T. Triantis, A. Hiskia, E. Papaconstantinou, Photocatalysis by polyoxometallates and TiO_2: a comparative study, Catalysis Today 124 (2007) 149–155.

[20] C. Chen, P. Lei, H. Ji, W. Ma, J. Zhao, Photocatalysis by titanium dioxide and polyoxometalate/TiO_2 cocatalysts. Intermediates and Mechanistic Study, Environmental Science & Technology 38 (2004) 329–337.

[21] R.R. Ozer, J.L. Ferry, Investigation of the photocatalytic activity of TiO_2–polyoxometalate systems, Environmental Science & Technology 35 (2001) 3242–3246.

[22] H. Lindstrom, H. Rensmo, S.-E. Lindquist, A. Hagfeldt, A. Henningsson, S. Sodergren, H. Siegbahn, Redox properties of nanoporous TiO_2 (anatase) surface modified with phosphotungstic acid, Thin Solid Films 323 (1998) 141–145.

[23] T. He, J. Yao, Photochromism in composite and hybrid materials based on transition-metal oxides and polyoxometalates, Progress in Materials Science 51 (2006) 810–879.

[24] U.L. Stangar, B. Orel, Chromogenic PWA/TiO_2 hybrid gels and films, Journal of Sol–Gel Science and Technology 8 (1997) 965–971.

[25] Z. Zhu, R. Tain, C. Rhodes, A study of the decomposition behaviour of 12-tungstophosphate heteropolyacid in solution, Canadian Journal of Chemistry 81 (10) (2003) 1044–1050.

[26] S.A. Bilmes, P. Mandelbaum, F. Alvarez, N. Victoria, Surface and electronic structure of titanium dioxide photocatalysts, Journal of Physical Chemistry B 104 (2000) 9851–9858.

[27] C. Kormann, D.W. Bahnemann, M.R. Hoffmann, Preparation and characterization of quantum-size titanium dioxide, Journal of Physical Chemistry 92 (18) (1988) 5196–5201.

[28] C.S. Kim, R.J. Lad, C.P. Tripp, Interaction of organophosphorous compounds with TiO_2 and WO_3 surfaces probed by vibrational spectroscopy, Sensors and Actuators B 76 (2001) 442–448.

[29] T. Oshima, K. Kondo, K. Ohto, K. Inoue, Y. Baba, Preparation of phosphorylated bacterial cellulose as an adsorbent for metal ions, Reactive and Functional Polymers 68 (2008) 376–383.

[30] G. Socrates, Infrared Characteristic Group Frequencies: Tables and Charts, 3rd ed., John Wiley and Sons, England, 2001278–323.

[31] A.N. Murashkevich, A.S. Lavitskaya, T.I. Barannikova, I.M. Zharskii, Infrared absorption spectra and structure of TiO_2–SiO_2, Applied Spectroscopy 75 (5) (2008) 730–734.

[32] A.J. Bridgeman, Density functional study of the vibrational frequencies of α-Keggin heteropolyanions, Chemical Physics 287 (2003) 55–69.

[33] H.-D. Wu, I.-D. Wu, F.-C. Chang, The interaction behavior of polymer electrolytes composed of poly(vinyl pyrrolidone) and lithium perchlorate ($LiClO_4$), Polymer 42 (2001) 555–562.

[34] A. Pearson, S.K. Bhargava, V. Bansal, UV-switchable polyoxometalate sandwiched between TiO_2 and metal nanoparticles for enhanced visible and solar light photococatalysis, Langmuir 27 (2011) 9245–9252.

[35] G.R. Hearne, J. Zhao, A.M. Dawe, V. Pischedda, M. Maaza, M.K. Nieuwoudt, P. Kibasomba, O. Nemraoui, J.D. Comins, Effect of grain size on structural transitions in anatase TiO_2: a Raman spectroscopy study at high pressure, Physical Review B 70 (2004) 134102–134110.

[36] T. Oshaka, F. Izumi, Y. Fujiki, Raman spectra of anatase, TiO_2, Journal of Raman Spectroscopy 7 (6) (1978) 321–324.

[37] H.C. Choi, Y.M. Jung, S.B. Kim, Size effects in the Raman spectra of TiO_2 nanoparticles, Vibrational Spectroscopy 37 (2005) 33–38.

[38] S.P.S. Proto, P.A. Fleury, T.C. Damen, Raman spectra of TiO_2, MgF_2 ZnF_2, FeF_2, and MnF_2, Physical Review 154 (2) (1967) 522–526.

[39] H.S. Barud, R.M.N. Assuncao, M.A.U. Martines, J. Dexpert-Ghys, R.F.C. Marques, Y. Messaddeq, S.J.L. Ribeiro, Bacterial cellulose–silica organic–inorganic hybrids, Journal of Sol-Gel Science and Technology 46 (2008) 363–367.

[40] I. Djerdj, A.M. Tonejc, Structural investigations of nanocrystalline TiO_2 samples, Journal of Alloys and Compounds 413 (2006) 159–174.

[41] X. Bokhimi, A. Morales, F. Pedraza, Crystallography and crystallite morphology of rutile synthesized at low temperature, Journal of Solid State Chemistry 169 (2002) 176–181.

[42] G.M. Brown, M.R. Noe-Spirlet, W.R. Busing, H.A. Levy, Dodecatungstophosphoric acid hexahydrate, $(H_5O_2^+)_3(PW_{12}O_{40}^{3-})$: the true structure of Keggin's 'pentahydrate' from single-crystal X-ray and neutron diffraction data, Acta Crystallographica B 33 (1977) 1038–1046.

[43] K.J.A Raj, R. Shanmugam, R. Mahalakshmi, B. Viswanathan, XPS and IR spectral studies on the structure of phopshata and sulphate modified titania—a combined DFT and experimental study, Indian Journal of Chemistry 49A (2010) 9–17.

[44] J.C. Edwards, C.Y. Thiel, B. Benac, J.F. Knifton, Solid-state NMR and FT-IR investigation of 12-tungstophosphoric acid on TiO_2, Catalysis Letters 51 (1998) 77–83.

[45] P.H. Lo, W.T. Tsai, J.T. Lee, M.P. Hung, Behavior of electroless plated Ni–P alloys in concentrated NaOH solution, Journal of the Electrochemical Society 142 (1995) 91–96.

[46] U.P. Rodrigues-Filho, Y. Gushikem, F.Y. Fujiwara, Zirconium dioxide supported on a-cellulose: synthesis and characterization, Langmuir 10 (1994) 4357–4360.

[47] G. Beamson, D. Briggs, High Resolution XPS of Organic Polymers, Wiley, Chichester, 1992158.

[48] S. Saliman, M. Delfino, Removal of native silicon oxide with low-energy argon ions, Journal of Applied Physics 70 (1991) 3970–3972.

[49] P.A. Jalil, M. Faiz, N. Tabet, N.M. Hamdan, Z. Hussain, A study of the stability of tungstophosphoric acid, $H_3PW_{12}O_{40}$, using synchrotron XPS, XANES, hexane cracking, XRD, and IR spectroscopy, Journal of Catalysis 217 (2003) 292–297.

[50] W. Grunert, R. Feldhaus, K. Anders, E.S. Shpiro, G.V. Antoshin, K.H.M. Minachev, A new facility for inert transfer of reactive samples to XPS equipment, Journal of Electron Spectroscopy and Related Phenomena 40 (1986) 187–192.

[51] C.D. Wagner, D.A. Zatko, R.H. Raymond, Journal of Analytical Chemistry 52 (1980) 1445 http://srdata.nist.gov/xps/XPSDetailPage.aspx?AllDataNo=21266

[52] M. Yoon, J.A. Chang, Y. Kim, J.R. Choi, Heteropoly acid-incorporated TiO_2 colloids as novel photocatalytic systems resembling the photosynthetic reaction center, Journal of Physical Chemistry B 105 (2001) 2539–2545.

[53] E.Q. Adaus, L. Osbnstein, The color and ionization of crystal-violet, Journal of the American Chemical Society 36 (7) (1914) 1452–1473.